

Information-Thermodynamic Analysis of the DNA–RNA Polymerase Complex via Interface Dissipation: Based on Observer–Observed Swap Symmetry

Tatsuaki Tsuruyama^{1,2,*}

¹Department of Physics, Tohoku University, Sendai 980-8578, Japan

²Department of Drug Discovery Medicine, Kyoto University, Kyoto 606-8501, Japan

(Dated:)

RNA polymerase (RNAP) elongates RNA by walking along a DNA template and selectively incorporating ribonucleoside triphosphates (rNTPs). Rather than mechanically replicating the base sequence, RNAP conditions binding and chemistry on the currently read template nucleotide, converting sequence dependence into a bias in its stochastic motion. Thermal fluctuations generate forward/backward translocation attempts; cognate rNTP binding and incorporation stabilize the forward register and suppress backward return, yielding net advance via a Brownian-ratchet mechanism.

We formulate the DNA–RNAP complex as a bipartite stochastic system, separating template-side degrees of freedom X from RNAP-side response degrees of freedom Y . Irreversibility is quantified by a Kullback–Leibler divergence between forward and time-reversed path measures, yielding joint and marginal dissipations. From these we define an exchange-invariant interface dissipation Σ_{int} that isolates time-reversal asymmetry generated specifically by coupling across the DNA–RNAP interface. We prove an exchange-symmetric second law, $\Sigma_{\text{int}} \geq 0$, and show that this interface measure is well defined without invoking local detailed balance.

To connect the framework to data analysis, we present a minimal continuous-time Markov jump model implementing the Brownian-ratchet logic and a likelihood-ratio protocol to estimate dissipation rates from discretely sampled trajectories. Finite-sample convergence is assessed via Markov-order diagnostics, clarifying bias–variance tradeoffs under coarse-graining. The interface-centered measure provides a consistent basis for comparing energetic cost across regimes (sequence-dependent kinetics, misincorporation, backtracking, proofreading) and can be combined with hidden-state inference when internal states are partially observed.

I. INTRODUCTION

A. RNAP and information thermodynamics: positioning relative to previous work

RNA polymerase (RNAP) is an enzyme that moves along DNA base by base (or by effective steps), incorporates the corresponding ribonucleotides, and elongates the RNA chain in the $5' \rightarrow 3'$ direction. Single-molecule experiments have allowed high-time resolution observations of RNAP’s stepwise motion, pauses, and backward excursions (backtracking), accelerating quantitative progress on the mechanistic and thermodynamic costs of transcription elongation ([1–6]).

A central viewpoint of information thermodynamics is that a Maxwell-demon-like mechanism is not necessarily an external controller: the same physical system can both acquire information about an input and use it to bias its own subsequent dynamics. RNAP provides a concrete molecular realization of this idea. By conditioning binding and chemical reactions on the currently read template base, RNAP converts sequence information into a directional bias of its own stochastic motion: thermal forward/backward translocation attempts are continuously

gated by base-dependent rNTP selection and incorporation, so that correct incorporation stabilizes the forward register and suppresses backward return, yielding rectified forward advance.

A previous study [7] presented an information-thermodynamic picture in which RNAP reads the base identity of the template DNA (X), selects and incorporates the complementary rNTP into the transcription complex and uses this as feedback to bias the subsequent dynamics (suppressing backward motion). Specifically, the template DNA side and RNAP side are represented by $X(m, d, N_m)$ and $Y(m, d, N_m)$, respectively, where

m : coordinate (register) of the bound RNAP,

$d \in \{+1, -1\}$: direction label, (1)

$N_m \in \{A, C, G, T\}$: template base at register m .

A , C , G , and T denote the DNA bases adenine, cytosine, guanine, and thymine. In this paper, we choose the transcription coordinate m so that elongation of the RNA by one nucleotide corresponds to $m \mapsto m + 1$. We define the RNAP direction label $d \in \{+1, -1\}$ by

$d = +1 : m \rightarrow m + 1$ (forward; elongation direction),
 $d = -1 : m \rightarrow m - 1$ (backward; backtracking direction). (2)

With this convention, for $d = +1$ RNAP moves along template DNA in the $3' \rightarrow 5'$ direction, while RNA

* tsuruyam@kuhp.kyoto-u.ac.jp

elongates in the $5' \rightarrow 3'$ direction. During elongation, RNAP holds the nascent RNA and the RNA–DNA hybrid within the transcription bubble constrains mechanical fluctuations. This constraint suppresses backward motion ($d = -1$) and can introduce additional kinetic barriers for backtracking. In minimal models, such effects are incorporated into transition-rate asymmetries via effective free-energy differences or directly via forward/backward rate ratios, while allowing refinements by state-space extension when needed.

In information thermodynamics, bookkeeping of information and dissipation can depend on how one partitions the system into a device (observer) and a target (observed system). In RNA synthesis, the observer and observed system are exchangeable in principle, yet most information-thermodynamic decompositions (e.g., learning rates or information-flow terms) are not invariant under exchanging the roles of measuring and measured subsystems. This motivates the search for quantities and constraints that remain well-defined under an observer–observed swap.

In this paper, X_t and Y_t denote the DNA-side and RNAP-side degrees of freedom, respectively. Depending on the modeling resolution, X_t may include the template register and base identity (e.g. $X_t = (m_t, N_{m_t})$), whereas Y_t may include RNAP mechanochemical states relevant for response (e.g. direction label, binding/locked states, etc.). When we use the schematic notation $X(m, d, N_m)$ and $Y(m, d, N_m)$, it is meant as a bookkeeping device indicating that both sides can be indexed by the same coarse register information, while their physical degrees of freedom are distinguished by the partition X vs. Y defined above.

B. This work: swap-invariant interface dissipation and an exchange-symmetric second law

The goal of this work is to formulate a swap-invariant measure of irreversibility for the coupled DNA–RNAP complex and to provide an operational route to estimate it from trajectory data. We quantify irreversibility using the path-space Kullback–Leibler (KL) divergence between the forward path measure and its time reversal. From the joint dissipation Σ_{XY} and the marginal dissipations Σ_X, Σ_Y obtained by projecting onto X or Y , we define the *interface dissipation*

$$\Sigma_{\text{int}} := \Sigma_{XY} - \frac{1}{2} (\Sigma_X + \Sigma_Y), \quad (3)$$

which is invariant under exchanging $X \leftrightarrow Y$. A central result of the present paper is an *exchange-symmetric second law*:

$$\Sigma_{\text{int}} \geq 0, \quad (4)$$

showing that the irreversibility generated specifically by coupling across the DNA–RNAP interface is nonnegative. Importantly, this result is derived at the level of

path measures and does not invoke local detailed balance (LDB), so it remains meaningful under coarse-graining where thermodynamic interpretations of rate ratios may fail.

To connect this framework to RNAP, we introduce a minimal continuous-time Markov jump process (CTMC) implementing the Brownian-ratchet logic: thermal forward/backward translocation attempts are rectified by base-dependent rNTP binding and incorporation that lock in forward progress. We then outline a likelihood-ratio protocol to estimate joint, marginal, and interface dissipation rates from discretely sampled trajectories. Because coarse-graining can render marginal dynamics non-Markovian, we include Markov-order diagnostics that expose a bias–variance tradeoff and justify adopting low-order estimators for robust quantitative comparisons.

C. Outline

Section II introduces the one-nucleotide stepping picture and the notation for thermodynamic parameters. Section III specifies the minimal CTMC model and defines the KL-based dissipations and the interface measure. Section III D presents practical estimators and convergence diagnostics based on Markov order r . Section IV discusses implications for RNAP energetics under sequence dependence, misincorporation, backtracking, and proofreading, and clarifies how swap-invariant interface dissipation complements conventional information-thermodynamic decompositions.

II. RNAP TRANSCRIPTION AND ONE-NUCLEOTIDE STEPPING: CONCEPTUAL MODEL AND NOTATION

A. Notation and thermodynamic parameters

Throughout, the template-base identity in the m register is denoted by $N_m \in \{A, C, G, T\}$. When a base-dependent quantity is evaluated at the next register, we write it as a function of N_{m+1} . We set the inverse temperature as $\beta := (k_B T)^{-1}$, where k_B is the Boltzmann constant, and T is the absolute temperature.

In the minimal CTMC, $k_+(m)$ and $k_-(m)$ denote thermal forward/backward translocation rates between registers m and $m + 1$. We parameterize their ratio by a structural free-energy difference (possibly dependent on base) $\Delta G_{\text{struct}}(N_m, N_{m+1})$ via $\ln[k_+(m)/k_-(m)] = -\beta \Delta G_{\text{struct}}(N_m, N_{m+1})$, and use a reference attempt rate k_0 in Eq. (9).

For rNTP binding, $k_{\text{on}}(N_{m+1})$ and $k_{\text{off}}(N_{m+1})$ are the (effective) binding/unbinding rates of the cognate rNTP complementary to the next template base. The factor $c_{N_{m+1}}$ is proportional to the concentration (or activity) of the solution of the cognate rNTP. $\Delta G_{\text{bind}}(N_{m+1})$ is

the corresponding contribution of binding free-energy in the effective coarse-grained description.

For the chemical locking step, $k_{\text{pol}}(N_{m+1})$ denotes the forward polymerization (incorporation) rate and $k_{\text{depol}}(N_{m+1})$ its minimal reverse reaction rate. $\Delta\mu_{\text{chem}}$ denotes the driving potential chemical associated with the release of NTP hydrolysis/pyrophosphate (or an equivalent effective driving), and $\Delta G_{\text{chem}}(N_{m+1})$ allows for base-dependent chemical contributions at the resolved level.

B. One-nucleotide stepping picture (Brownian-ratchet viewpoint)

RNAP advances along the template DNA through thermal forward/backward fluctuations while selectively recruiting and incorporating the rNTP complementary to the currently read template base. The key point of the Brownian-ratchet viewpoint is that chemical events do not directly push RNAP mechanically; rather, they *lock in* a forward-advanced configuration and suppress ineffective backward return, thereby rectifying fluctuations into net forward progress.

Figure 1 summarizes the one-nucleotide stepping cycle used throughout this paper. Panel (A) illustrates *recruitment*: at register m , RNAP reads the next template base and recruits an rNTP to the active site. Panel (B) shows *hybridization*: the recruited cognate rNTP forms a correct base pair within the transcription bubble, stabilizing the forward register. Panel (C) shows *elongation (incorporation)* at the 3' end of the RNA, extending the RNA–DNA hybrid by one nucleotide (chemical locking). Panel (D) shows *translocation*: RNAP shifts the reaction field from m to $m+1$ by one nucleotide (step length Δ), completing the cycle and preparing the next recruitment.

III. MINIMAL BROWNIAN-RATCHET MODEL: A CTMC FOR SIMULATION

In this section, as a mathematically rigorous continuous-time Markov jump process (CTMC), we formulate a minimal model that captures the Brownian-ratchet mechanism emphasized in [7]: RNAP undergoes spontaneous forward/backward fluctuations, and correct-rNTP binding and polymerization rectify those fluctuations by suppressing ineffective backward return, yielding net forward motion. Importantly, we do not assume that rNTP hydrolysis mechanically pushes RNAP forward; rather, chemical reactions *capture* favorable thermal fluctuations.

We emphasize that the internal-state description introduced below is not meant to be biochemically exhaustive; it is the minimal coarse-grained scaffold needed to (i) implement the Brownian-ratchet logic and (ii) make the path-space KL definitions and estimators explicit.

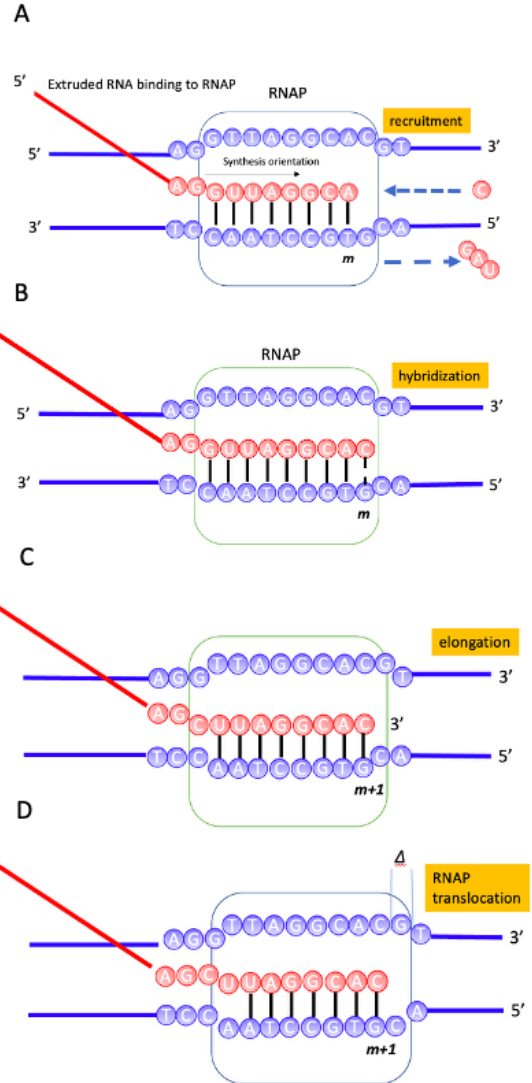


FIG. 1. One-nucleotide stepping cycle of transcription by RNAP, consistent with the notation in the main text. Blue lines/circles represent the DNA duplex (template track), and red lines/circles represent the nascent RNA (5' \rightarrow 3' elongation). The rounded box indicates the transcription bubble / reaction field in which base selection, hybridization, and chemistry occur. The coordinate m labels the RNAP register before the step and $m+1$ after the step; the symbol Δ denotes the translocation distance of a single-nucleotide step (chosen to avoid collision with the direction label $d \in \{\pm 1\}$ used in the text).

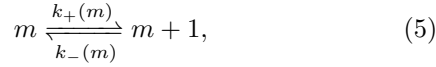
a. Minimal internal state on the RNAP side. To make the CTMC specification explicit while keeping the model minimal, we introduce an RNAP-side internal state $s_t \in \{0, 1, 2\}$: $s_t = 0$ (no rNTP bound; pre-binding), $s_t = 1$ (cognate rNTP bound / hybridized), and $s_t = 2$ (chemically locked after incorporation). We take $Y_t := s_t$. The DNA-side variable X_t is the register-

dependent template input, which we represent as the pair (m_t, N_{m_t+1}) (equivalently, m_t together with the fixed sequence $\{N_m\}$). With this choice, the process is bipartite: each jump changes either m_t (hence X_t) or s_t (hence Y_t), but not both.

A. Transition classes and rates (generator specification)

We define a CTMC on the state space of $Z_t := (X_t, Y_t)$. Transitions fall into three classes.

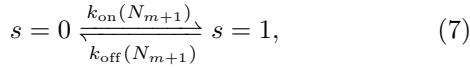
a. (i) *Spontaneous translocation fluctuations (thermal steps)*. RNAP performs thermal forward/backward steps,



with a structural asymmetry absorbed into a free-energy difference ΔG_{struct} :

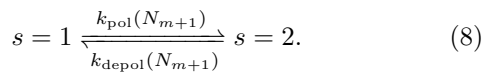
$$\ln \frac{k_{+}(m)}{k_{-}(m)} = -\beta \Delta G_{\text{struct}}(N_m, N_{m+1}). \quad (6)$$

b. (ii) *Binding/unbinding of the cognate rNTP (RNAP-side chemical state changes)*. With the register fixed, the RNAP-side state s switches between 0 and 1:



where the base dependence enters through the next template base N_{m+1} .

c. (iii) *Chemical locking (polymerization) and its minimal reverse reaction*. With the register fixed, chemical incorporation changes s between 1 and 2:



The reverse reaction is included only to keep the path-space KL divergence well-defined for a CTMC; in regimes of strong chemical driving one typically has $k_{\text{depol}} \ll k_{\text{pol}}$.

B. Concrete parametrization of transition rates

For notational convenience in Eqs. (10)–(11), we write $X := N_{m+1}$ for the next template base.

a. (i) *Thermal steps (structural free-energy difference)*.

$$\begin{aligned} k_{+}(m) &= k_0 \exp \left[-\frac{\beta}{2} \Delta G_{\text{struct}}(N_m, N_{m+1}) \right], \\ k_{-}(m) &= k_0 \exp \left[+\frac{\beta}{2} \Delta G_{\text{struct}}(N_m, N_{m+1}) \right]. \end{aligned} \quad (9)$$

This enforces Eq. (6) exactly.

b. (ii) *Binding/unbinding of the correct rNTP (depends on $X = N_{m+1}$)*.

$$\begin{aligned} k_{\text{on}}(X) &= k_{\text{on}}^0 c_X, \\ k_{\text{off}}(X) &= k_{\text{off}}^0 \exp[+\beta \Delta G_{\text{bind}}(X)], \end{aligned} \quad (10)$$

where $c_X \propto [\text{rNTP}(X)]$ denotes the concentration (activity) of the cognate rNTP species complementary to X .

c. (iii) *Polymerization (locking) and the reverse reaction (depolymerization)*. To define the path-space KL rigorously, include a minimal reverse reaction:

$$\begin{aligned} k_{\text{pol}}(X) &= k_{\text{pol}}^0 \exp[-\beta \Delta G_{\text{act}}(X)], \\ k_{\text{depol}}(X) &= k_{\text{pol}}(X) \exp[-\beta(\Delta \mu_{\text{chem}} - \Delta G_{\text{chem}}(X))]. \end{aligned} \quad (11)$$

In regimes where the reverse reaction is negligible, one may take $k_{\text{depol}}(X) \ll k_{\text{pol}}(X)$.

C. Definitions of observables

Let P_{XY} be the forward path measure of the composite system (X, Y) on a fixed time window $[0, T]$. We define the time-reversed path measure via the time-reversal map \mathcal{R} by

$$P_{XY}^{\text{R}} := P_{XY} \circ \mathcal{R}^{-1}. \quad (12)$$

Here \mathcal{R} reverses the temporal order of a trajectory (and, if needed, applies the appropriate state-space involution; in the present setting we focus on temporal reversal of sample paths). We define irreversibility (dissipation) primarily as the path-space KL divergence

$$\Sigma_{XY} := D_{\text{KL}}(P_{XY} \parallel P_{XY}^{\text{R}}) = \int \log \left(\frac{dP_{XY}}{dP_{XY}^{\text{R}}} \right) dP_{XY}. \quad (13)$$

This definition is purely probabilistic and does not assume local detailed balance (LDB). For CTMC models, Σ_{XY} coincides with the expected log-likelihood ratio between the forward and reversed path ensembles and can be estimated from trajectories as discussed below.

Let the projections be $\Pi_X(X, Y) = x$ and $\Pi_Y(X, Y) = y$, and define

$$P_X := \Pi_X P_{XY}, \quad P_Y := \Pi_Y P_{XY}, \quad (14)$$

and

$$P_X^{\text{R}} := \Pi_X P_{XY}^{\text{R}}, \quad P_Y^{\text{R}} := \Pi_Y P_{XY}^{\text{R}}. \quad (15)$$

Then the marginal dissipations are

$$\Sigma_X := D_{\text{KL}}(P_X \parallel P_X^{\text{R}}), \quad \Sigma_Y := D_{\text{KL}}(P_Y \parallel P_Y^{\text{R}}). \quad (16)$$

By the data-processing inequality, $\Sigma_{XY} \geq \Sigma_X, \Sigma_Y$.

Definition 1 (Interface dissipation).

$$\Sigma_{\text{int}} := \Sigma_{XY} - \frac{1}{2} (\Sigma_X + \Sigma_Y). \quad (17)$$

Theorem 2 (Exchange-symmetric second law). *Assume that the conditional path measures $P_{Y|X}$ and $P_{X|Y}$ exist for the forward and time-reversed ensembles. Then the interface dissipation defined in Eq. (17) is invariant under swapping $X \leftrightarrow Y$ and satisfies*

$$\Sigma_{\text{int}} \geq 0. \quad (18)$$

Proof. Since Σ_{int} depends on $(\Sigma_X + \Sigma_Y)$ symmetrically, invariance under $X \leftrightarrow Y$ is immediate. To prove non-negativity, use the chain rule of KL divergence. Writing $P_{XY} = P_X P_{Y|X}$ and $P_{XY}^R = P_X^R P_{Y|X}^R$, we obtain

$$\Sigma_{XY} = \Sigma_X + \int P_X(d\gamma) D_{\text{KL}}\left(P_{Y|X=\gamma} \parallel P_{Y|X=\gamma}^R\right), \quad (19)$$

hence $\Sigma_{XY} - \Sigma_X \geq 0$. Similarly, $\Sigma_{XY} - \Sigma_Y \geq 0$. Because $\Sigma_{\text{int}} = \frac{1}{2}[(\Sigma_{XY} - \Sigma_X) + (\Sigma_{XY} - \Sigma_Y)]$, we obtain the two-column-safe representation

$$\begin{aligned} \Sigma_{\text{int}} &= \frac{1}{2} \left[\int P_X(d\gamma) D_{\text{KL}}\left(P_{Y|X=\gamma} \parallel P_{Y|X=\gamma}^R\right) \right. \\ &\quad \left. + \int P_Y(d\eta) D_{\text{KL}}\left(P_{X|Y=\eta} \parallel P_{X|Y=\eta}^R\right) \right] \geq 0. \end{aligned} \quad (20)$$

□

Remark 3 (Interpretation). Equation (20) shows that Σ_{int} is an average of conditional KL gaps, hence a genuine inequality (law) rather than a definition. It isolates the irreversibility that cannot be attributed to either marginal alone and is generated specifically by coupling across the X - Y interface.

D. Convergence diagnostics and Markov order r

a. Discretized sequences. We discretize an observed continuous-time trajectory at a fixed sampling interval Δt and obtain $N + 1$ samples at times $t_n := n\Delta t$ ($n = 0, 1, \dots, N$), with total observation time $T_{\text{obs}} := N\Delta t$. To present the estimation procedure in a unified notation, we introduce a generic discrete sequence S_n :

$$S_n := \begin{cases} X_n, & \text{when estimating } \Sigma_X, \\ Y_n, & \text{when estimating } \Sigma_Y, \\ (X_n, Y_n), & \text{when estimating } \Sigma_{XY}. \end{cases} \quad (21)$$

Thus S_n is not an additional physical variable; it is a placeholder that selects the target observable alphabet.

b. Uppercase P vs. lowercase p . Let $P(\cdot)$ denote the probability law of the *entire* discretized sequence $S_{0:N} := (S_0, \dots, S_N)$ induced by sampling the continuous-time path at interval Δt . We use lowercase $p(\cdot | \cdot)$ for the corresponding *one-step conditional probabilities* in the chain rule:

$$P(S_{0:N}) = P(S_0) \prod_{n=0}^{N-1} p(S_{n+1} | S_{0:n}), \quad (22)$$

where $S_{0:n} := (S_0, \dots, S_n)$ is the history up to index n and $S_{a:b} := (S_a, S_{a+1}, \dots, S_b)$ is the shorthand for subsequences.

c. Definition of Markov order r . Because the marginal sequences (e.g. X_n or Y_n) are generally non-Markovian after coarse-graining, we approximate the history-dependent conditional probability by a finite memory length (context length) $r \in \mathbb{N}$:

$$p(S_{n+1} | S_{0:n}) \approx p^{(r)}(S_{n+1} | S_{n-r+1:n}), \quad (23)$$

where $S_{n-r+1:n}$ is a length- r context block. Thus $r = 1$ corresponds to a first-order Markov approximation $p(S_{n+1} | S_{0:n}) \approx p^{(1)}(S_{n+1} | S_n)$, while $r \geq 2$ incorporates longer history dependence.

d. Forward/reverse likelihood-ratio estimator (Markov(r)). Let $\tilde{S}_n := S_{N-n}$ denote the time-reversed discrete sequence. From the forward data $\{S_n\}$ and the reversed data $\{\tilde{S}_n\}$, construct empirical/parametric conditional probabilities $\hat{p}_F^{(r)}(\cdot | \cdot)$ and $\hat{p}_R^{(r)}(\cdot | \cdot)$. We then estimate the dissipation-rate (KL-rate) for the chosen observable S by

$$\hat{\Sigma}^{(r)}[S] := \frac{1}{N_{\text{eff}} \Delta t} \sum_{n=r-1}^{N-1} \ln \frac{\hat{p}_F^{(r)}(S_{n+1} | S_{n-r+1:n})}{\hat{p}_R^{(r)}(\tilde{S}_{n+1} | \tilde{S}_{n-r+1:n})}, \quad (24)$$

where $N_{\text{eff}} := N - (r - 1)$. Applying Eq. (24) to $S = X$, Y , and (X, Y) yields $\hat{\Sigma}_X^{(r)}$, $\hat{\Sigma}_Y^{(r)}$, and $\hat{\Sigma}_{XY}^{(r)}$, and we define the interface estimator by

$$\hat{\Sigma}_{\text{int}}^{(r)} := \hat{\Sigma}_{XY}^{(r)} - \frac{1}{2} \left(\hat{\Sigma}_X^{(r)} + \hat{\Sigma}_Y^{(r)} \right). \quad (25)$$

e. Larger r is not always better (bias-variance trade-off). Increasing r reduces modeling bias but increases estimation variance because the number of contexts grows rapidly (roughly as $|\mathcal{S}|^r$). This sparsity can cause strong finite-sample overestimation of log-likelihood ratios.

f. Practical handling in this paper. We use $r = 1$ as a stable reference estimator in the main figures and interpret behavior at $r \geq 2$ primarily as a diagnostic. The convergence trends are summarized in Figs. 2 and 3.

Figures 2 and 3 illustrate a typical finite-sample behavior of the Markov(r) likelihood-ratio estimators. For the interface-dissipation-rate estimate $\hat{\Sigma}_{\text{int}}^{(r)}$ [Fig. 2], the

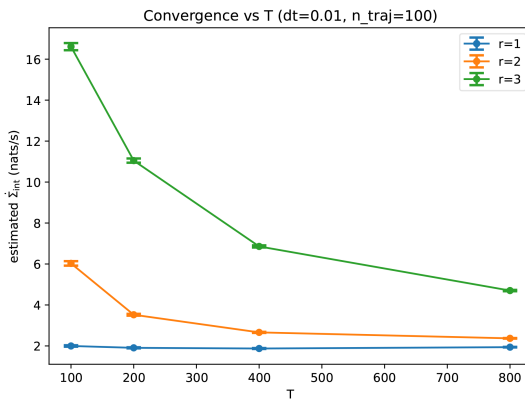


FIG. 2. Convergence diagnostics for the interface-dissipation-rate estimator (dependence on observation length T_{obs}). With fixed sampling interval Δt , estimate $\hat{\Sigma}_{\text{int}}^{(r)}$ for multiple Markov orders r and plot the mean estimate versus T_{obs} . The stability of $r = 1$ and the sensitivity of $r \geq 2$ to sparse estimation at finite data are illustrated.

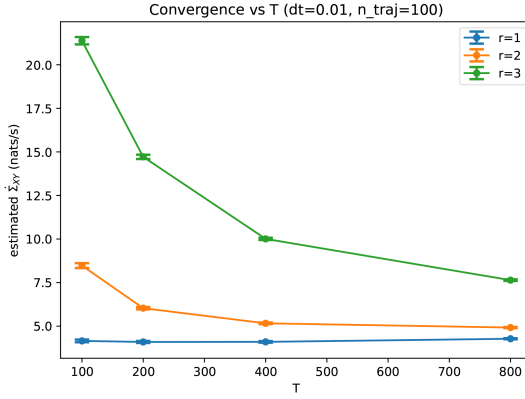


FIG. 3. Convergence diagnostics for the total dissipation-rate estimator (dependence on observation length T_{obs}). Under the same settings, estimate $\hat{\Sigma}_{XY}^{(r)}$ and compare across T_{obs} .

$r = 1$ curve is nearly flat already at the shortest observation window, staying around ~ 1.9 nats/s. In contrast, $r = 2$ and $r = 3$ show clear downward trends with increasing T_{obs} : for example, $r = 2$ decreases from ~ 6 to ~ 2.3 nats/s and $r = 3$ from ~ 17 to ~ 4.7 nats/s

over the range shown. The same tendency is even more pronounced for the total dissipation-rate estimate $\hat{\Sigma}_{XY}^{(r)}$ [Fig. 3], while $r = 1$ remains stable around ~ 4.1 nats/s.

This behavior is consistent with the standard bias-variance tradeoff for finite-context estimators: increasing r reduces modeling bias but rapidly increases the number of contexts (roughly $|\mathcal{S}|^r$), making many contexts poorly sampled at finite T_{obs} and leading to systematic overestimation of log-likelihood ratios. Accordingly, throughout the main text we adopt $r = 1$ as a robust reference estimator and use $r \geq 2$ primarily as a diagnostic of history dependence rather than as final quantitative values.

IV. DISCUSSION

In this setting, the swap-invariant interface dissipation Σ_{int} isolates the irreversibility generated specifically by DNA–RNAP coupling, filtering out time-asymmetry already present in either marginal description and avoiding ambiguity in assigning observer and observed roles. This KL-based formulation is particularly useful under experimental and model coarse-graining, where effective dynamics may be Markovian while local detailed balance at the observed level can be violated or untestable, rendering heat/entropy-production decompositions gauge dependent; by contrast, Σ_{XY} , Σ_X , Σ_Y , and Σ_{int} remain operational measures of time-reversal asymmetry, with mutual information serving only as an auxiliary diagnostic and with LDB-based interpretations applied only when justified. For data analysis, marginal projections typically induce memory, so dissipation-rate estimation benefits from finite-context (Markov- r) likelihood-ratio estimators and their convergence trends as robustness checks; when internal states are hidden, latent-state inference (e.g. HMMs) can be incorporated at the cost of additional model dependence, most strongly affecting marginal quantities such as Σ_Y . Extensions that are natural within the same bookkeeping include richer mechanochemical state spaces (pause/backtrack substates), explicit misincorporation and proofreading networks (e.g. incorporating a four-valued R_m and cleavage cycles), controlled forcing and concentration dependence, and systematic characterization of how Σ_X , Σ_Y , and Σ_{int} transform under changes of observational partition and temporal resolution.

[1] E. A. Abbondanzieri, W. J. Greenleaf, J. W. Shaevitz, R. Landick, and S. M. Block, Direct observation of base-pair stepping by RNA polymerase, *Nature* **438**, 460–465 (2005).

[2] P. Thomen, P. J. Lopez, U Bockelmann, J. Guillerez, M. Dreyfus, and S. M. Heslot, T7 RNA polymerase studied by force measurements varying cofactor concentration, *Biophys. J.* **95**, 2423–2433 (2008).

[3] L. Bai, R. M. Fulbright, and M. D. Wang, Mechanochemical kinetics of transcription elongation, *Phys. Rev. Lett.* **98**, 068103 (2007).

[4] L. Bai, A. Shundrovsky, and M. D. Wang, Sequence-dependent kinetic model for transcription elongation by RNA polymerase, *J. Mol. Biol.* **344**, 335–349 (2004).

[5] M. D. Wang, T. E. Elston, R. Landick, and S. M. Block, Force generation in RNA polymerase, *Science* **282**, 902–

907 (1998).

[6] Q. Guo and R. Sousa, Translocation by T7 RNA polymerase: a sensitively poised Brownian ratchet, *J. Mol. Biol.* **358**, 241–254 (2006).

[7] T. Tsuruyama, RNA polymerase is a unique Maxwell’s demon that converts its transcribing genetic information to free energy for its movement, *Eur. Phys. J. Plus* **138**, 604 (2023).

[8] T. Tsuruyama, Thermodynamics Reconstructed from Information Theory: An Axiomatic Framework via Information-Volume Constraints and Path-Space KL Divergence, arXiv:2512.24655 (2025).

[9] D. T. Gillespie, Exact stochastic simulation of coupled chemical reactions, *J. Phys. Chem.* **81**, 2340–2346 (1977).

[10] P. Pietzonka and U. Seifert, Universal trade-off between power, efficiency, and constancy in steady-state heat engines, *Phys. Rev. Lett.* **120**, 190602 (2018).

[11] U. Seifert, Stochastic thermodynamics, fluctuation theorems and molecular machines, *Rep. Prog. Phys.* **75**, 126001 (2012).

[12] J. Schnakenberg, Network theory of microscopic and macroscopic behavior of master equation systems, *Rev. Mod. Phys.* **48**, 571–585 (1976).

[13] J. L. Lebowitz and H. Spohn, A Gallavotti–Cohen-type symmetry in the large deviation functional for stochastic dynamics, *J. Stat. Phys.* **95**, 333–365 (1999).

[14] L. R. Rabiner, A tutorial on hidden Markov models and selected applications in speech recognition, *Proc. IEEE* **77**, 257–286 (1989).

[15] T. Tsuruyama, Thermodynamics of Information: Mutual Entropy in RNA Polymerase and Nanopore Sequencing, (Review manuscript / draft; see also related discussion in [7]).

[16] V. Tripathi, G. M. Schütz, and D. Chowdhury, Interacting RNA polymerase motors on a DNA track: effects of traffic congestion and intrinsic noise, *Phys. Rev. E* **79**, 011921 (2009).